1 of 9



Received: 30 September 2021 Accepted: 22 October 2021

# Electrochemically activated polyaniline based ambipolar organic electrochemical transistor

Hugo José Nogueira Pedroza Dias Mello<sup>1,2</sup> Murilo Calil Faleiros<sup>2</sup> Marcelo Mulato<sup>2</sup>

### Correspondence

Hugo José Nogueira Pedroza Dias Mello, Institute of Physics, Federal University of Goiás (UFG), Goiânia, GoiásGO 74690-900, Brazil.

Email: hugomello@ufg.br

### **Abstract**

The organic electrochemical transistors (OECTs) are largely applied as bio- and ion-sensor devices due to their performance in an aqueous environment with electrochemical doping/dedoping (reversible redox reactions) of the semiconducting layer through ion injection and also low (around 1 V) operation potentials. Aiming for the complementary circuits' development and improvement of the sensors device, we report the application of spin coated polyaniline (PANI) in ambipolar OECT. The OECT operation is based on electrochemical protonation/deprotonation of PANI upon applied gate potential that was verified by cyclic voltammograms (CV) of PANI sample. The device operates in accumulation mode with on-currents on the milliampere range due to the use of interdigitated array (IDA) microelectrodes architecture with a larger active area. Acid (HCl) doped PANI were applied in OECT device for comparison, and it presented improved performance with increasing drain-source current up to 38%, reaching 4.8 mA for the *n*-type device. This current increase is due to the narrower bandgap of doped PANI that affects the injection barrier. The HCl doped PANI was evaluated by UV-Vis spectrophotometry and CV analysis. Using deionized water as electrolyte defunctionalized the PANI-based OECT (no current modulation observed) because the absence of ions in the electrolyte interrupts the electrochemical doping. This is the opposite for the poly(3-hexylthiophene) (P3HT)based electrolyte-gated organic field-effect transistor (EGOFET) due to the polymeric hydrophobicity nature that allows for field-effect modulation in the electrolyte/semiconductor interface. The results presented may open new possibilities for bio- and ion-sensors devices.

### KEYWORDS

ambipolar, electrically conducting polymer, electrochemical doping, electrolyte-gated transistors, organic semiconductors, polyaniline

This is an open access article under the terms of the Creative Commons Attribution-NonCommercial-NoDerivs License, which permits use and distribution in any medium, provided the original work is properly cited, the use is non-commercial and no modifications or adaptations are made.

© 2021 The Authors. *Electrochemical Science Advances* published by Wiley-VCH GmbH.

<sup>&</sup>lt;sup>1</sup> Institute of Physics, Federal University of Goiás (UFG), Goiânia Goiás, Brazil

<sup>&</sup>lt;sup>2</sup> Department of Physics, Faculty of Philosophy, Sciences and Letters at Ribeirao Preto (FFCLRP), University of Sao Paulo (USP), Ribeirao Preto, Sao Paulo, Brazil

Research article

doi.org/10.1002/elsa.202100176

#### INTRODUCTION 1

Transistors are semiconductor devices first proposed by Lilienfeld in 1930.<sup>[1]</sup> Lilienfeld discussed the basis of a field-effect transistor (FET) device. Basically, an FET operates as a parallel plate capacitor with one of the plates as the conductive channel where current flows between two contacts, drain (D) and source (S), the drain-source current,  $I_{DS}$ , due to the application of an electrical polarity, the drain-source potential,  $V_{\rm DS}$ . The charge carrier density is modulated by the potential applied to the other plate, the gate (G), the gate-source potential,  $V_{GS}$ . The first FET structure with semiconducting silicon-based metal oxides is the metal-oxide-semiconductor FET (MOSFET).[2]

Modern applications required the transistors devices to be miniaturized, with low cost and presenting tailored properties. The use of thin-film transistor (TFT) technology allows for overcoming these needs.[3] Not only the cited properties but also the need for flexibility and biointegration give rise to the area of organic materials applied to electronics with the use of organic semiconductors (OSC) in organic TFT (OTFT) devices. [4,5] The now miniaturized device has to be able to operate with high-density electronic carriers and low operational voltage that is achieved by the use of electrolyte as dielectric in transistors giving rise to the electrolyte-gated transistors (EGT).<sup>[6]</sup> Such devices can operate with low voltages and high-density charge accumulation due to the formation of electric double layer capacitors (EDLC) in the electrolyte/semiconductor interface and in the gate electrode/electrolyte interface.[7]

An EGT based on an OTFT architecture consists of an OSC layer in contact with an electrolyte, in which the gate electrode is immersed and it works as a combination of field-effect and doping process occurring mutually.<sup>[8]</sup> However, with the correct applied potential range and semiconducting layer, the device may operate as a FET system or based on electrochemical doping.[9] The first class of devices are the electrolyte-gated organic FET (EGOFET), [10-13] which have presented stable operation in aqueous environment.[14] Devices operating with electrochemical doping, that is, ion injection into the semiconducting layer from the electrolyte, are the organic electrochemical transistors (OECT) that work based on the doping/dedoping of an electrically conducting polymer (ECP), a class of OSC, which results in the modification of its conductivity.[15-18] These devices operate in aqueous environment and can efficiently transduce ionic signals into electrical ones being applied as OFET<sup>[19-24]</sup> and OECT<sup>[25-29]</sup> bio- and ion-sensors.

The model proposed for EGTs devices follow the classical derivation for the inorganic with solid dielectric MOSFET<sup>[30]</sup> and is based on the drift of accumulated charge in the channel obtained either by field-effect phenomenon or by electrochemical doping for the EGOFET and OECT, respectively. The current model for EGOFETs is the same as for MOSFETs.<sup>[31]</sup> For OECT, the model was proposed by Bernards and Malliaras in 2007,[32] by coupling an electronic circuit, composed of drain-ECP-source, with an ionic circuit, composed of gate-electrolyte-ECP. The OECT current modulation model can be expressed as:

$$I_{DS} = \frac{W \cdot T}{L} \cdot \mu \cdot C^* \cdot \left[ V_{GS} - V_{Th} - \frac{V_{DS}}{2} \right] \cdot V_{DS} \quad (1)$$

In Equation (1),  $\mu$  is the charge mobility,  $C^*$  is the capacitance per volume, L is the channel length, distance between the drain and source electrodes, W is the channel width, the size of the contacts perpendicular to the  $I_{DS}$ , T is the channel thickness, and  $V_{Th}$  is the threshold voltage, that is, the onset of the device. In OECT, the electrochemical doping/dedoping of the channel material occurs at any spatial position, that is, it is not limited to the channel interface, justifying the capacitance per volume.[33]

Most OECT devices have a unipolar operation, that is, only holes or electrons as charge carriers, being of p- or ntype channel. Ambipolarity would be achieved with materials presenting high electron and hole mobility,  $\mu$ , to sustain electronic currents as predicted by Equation (1). Therefore, ambipolar OECTs would allow the complementary circuits development and improvement of the bioelectronic devices. As for ambipolar OFETs, [34] ambipolar OECTs is one with channel formation with both holes and electrons. The achievement of ambipolar OECTs depends on the development of appropriate semiconducting materials which has the need of presenting both stability in an aqueous environment and reversible redox reaction, oxidation and reduction, for electrochemical doping/dedoping of the semiconducting layer in the appropriate potential window.[35]

Among many organic materials used in organic electronics, polyaniline (PANI), a conjugated polymer, has been applied in OFETs<sup>[36-38]</sup> and OECTs<sup>[39-41]</sup> devices. Besides that, it is a first candidate for ambipolar OECT once it is stable in an aqueous environment and also presents reversible redox reaction in the electrochemical window causing electrochemical doping/dedoping, that is, injection of cations and anions from the electrolyte, enabling its ionic conduction.[42-46] Solid-state ambipolar PANI-based devices were reported. They work based on gate voltage induced n- and p-type doping using positive and negative mobile ions either using a polymeric electrolyte, poly(ethyleneimine) (PEI), with excess of cations deposited over PANI-camphor sulfonic acid (PANI-CSA) layer [47] or a poly(vinyl alcohol) (PVA) layer deposited over PANI-poly(styrene sulfonic acid) (PANI-PSS) layer, [48]

Chemistry Europe

European Chemical Societies Publishing

both acting as channel layer in the transistor. In the EGT architecture, the doping process changes and the PANI layer undergoes ion injection from the electrolyte upon application of an appropriate gate potential in an electrochemical doping/dedoping process. In this work, we report an ambipolar PANI-based OECT fabricated with interdigitated array (IDA) microelectrodes substrate operating in buffer solution through electrochemical doping/dedoping process, comparing its performance to strong acid doped PANI-based OECT and to poly(3-hexylthiophene) (P3HT)-based EGOFET, opening new possibilities for bio- and ionsensors devices.

### 2 | MATERIALS AND METHODS

### 2.1 | Sample device preparation

The OECT devices were fabricated using IDA microelectrodes (Als. Co, Tokyo, Japan) fabricated by lithography comprising a quartz glass substrate with gold source, drain, and gate electrodes (electrode length of 10 µm, channel length L = 5  $\mu$ m, channel width W = 2 mm, and 65 pairs). After cleaning by ultrasonication in deionized (DI)-water, ethanol and acetone (5 min each), and drying in air, emeraldine base PANI (PANI-EB) (Sigma Aldrich, M<sub>W</sub> 50,000 g/mol) was deposited from a weight ratio of 1:100 polymer:solvent N,N-Dimethylformamide (DMF) (Synth) solution (PANI:DMF OECT).[49] For the doped PANI, HCl (Sigma Aldrich) was added to the precursor PANI solution in a polymer:solvent:dopant ratio 1:100:1.5 (PANI:DMF:HCl OECT). Both solutions were mixed by stirring for 1 h and ultrasonicated for 1 h at room temperature, that is, 298 K. The EGOFET device was fabricated from a 5 mg/mL ((0.5 wt.%) regioregular P3HT (Rieke Metals,  $M_W = 37,000 \text{ g/mol}$ , 98% regioregular) chlorobenzene solution mixed by stirring overnight (400 rpm). All devices were deposited via spin-coating (1000 rpm, for 60 s) and the samples were annealed on a hot plate for 20 min at 120°C.

### 2.2 | Device characterization

Electrical characterization was performed in air with the devices connected to an Agilent system (34970A data acquisition/switch unit and E3646A dual output DC power supply) controlled via a home-written LabVIEW program, measuring the output and transfer characteristics of the devices by scanning the potential between drain and source ( $V_{\rm DS}$ ) and the potential between gate and source ( $V_{\rm GS}$ ), respectively, measuring the current between drain and source ( $I_{\rm DS}$ ). A platinum (Pt) rod ( $\emptyset$  = 1.0 mm, L = 25 mm) was used as the external gate electrode. For

the OECT device, a 0.5 mol/L sodium phosphate buffer (PB) (composed of anhydrous dibasic sodium phosphate (P.A.-A.C.S. Synth, 99.5%) and sodium phosphate monobasic (P.A.-A.C.S. Synth, 99.5%)) was used as electrolyte. For device operation mode analysis and the EGOFET device, DI-water (DI-W) was used as an electrolyte. All experiments were performed at room temperature, that is, 298 K.

### 2.3 | Electrochemical measurements

Cyclic voltammetry (CV) method was applied by using an AUTOLAB potentiostat (Metrohm) with an FRA module controlled by the software NOVA. A conventional three-electrode system was used. The working electrode was PANI thin film samples (PANI:DMF and PANI:DMF:HCl) prepared as for the OECT devices over fluorine tin-oxide (FTO) (Sigma-Aldrich) substrates cleaned by ultrasonication in DI-water, ethanol, and acetone (10 min each). The reference electrode was an AglAgCl electrode and a platinum foil was used as a counter electrode. All experiments were performed at room temperature, that is, 298 K.  $\rm H_2SO_4$  aqueous solution (0.5 mol/L) was applied as a supporting electrolyte with a scan rate of 50 mV/s from – 0.2 to 1.2 V (vs. AglAgCl).

## 2.4 | UV-Vis spectrophotometry measurement

The UV-Vis optical spectra of the PANI deposition solution (PANI:DMF and PANI:DMF:HCl) were recorded using a Ultrospec™ 2100 pro (Amersham Pharmacia) in absorbance mode, from 270 to 900 nm with a wavelength rate of 750 nm/min, in a 1 nm step. All experiments were performed at room temperature, that is, 298 K.

### 3 | RESULTS AND DISCUSSION

The bottom contact PANI-EB-based OECT device is illustrated in Figure 1a with the Pt rod gate electrodes biasing the transistors in an aqueous environment (the same structure is valid for the EGOFET device with the P3HT as OSC layer). The device's array of microelectrodes is shown in the optical microscopy image in Figure 1b. The OECT possess 65 pairs of drain-and-source channels, with a 5  $\mu$ m channel length and a 2 mm channel width each.

The IDA microelectrode based OECT performance is presented in Figure 2. The output curves ( $I_{DS}$  versus  $V_{DS}$ ) for both drain-source applied polarity, positive and negative, of the PANI OECT device are presented in Figure 2a,

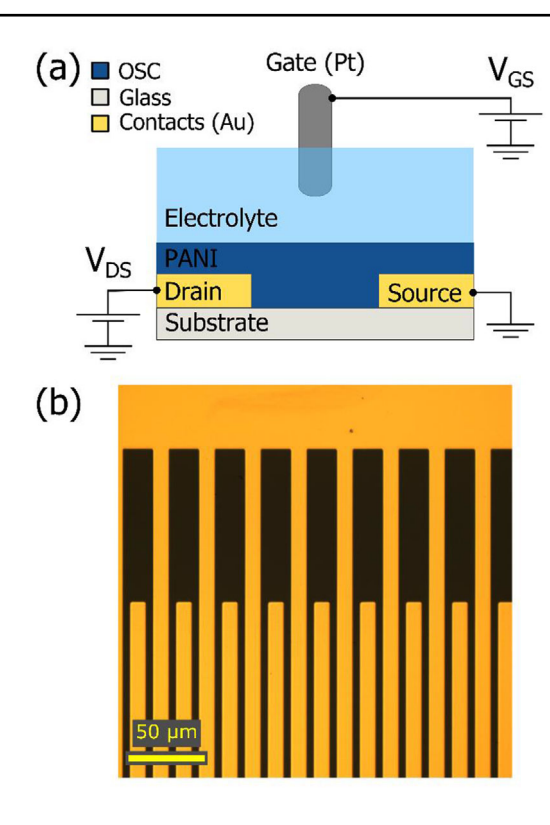


FIGURE 1 Cross-section schematic of an organic electrochemical transistor (OECT) using polyaniline (PANI) as the organic semiconductor (OSC) layer based on a bottom contact interdigitated array (IDA) microelectrode substrate in panel (a). A platinum (Pt) rod was used as an external gate electrode. An optical microscopy image of the IDA electrode in (b). The yellow printed side is the electrode with length 10  $\mu$ m. The intercalated electrodes are the drain and source array

and c, respectively, and the transfer curves ( $I_{\rm DS}$  versus  $V_{\rm GS}$ ) are presented in Figure 2b and d, respectively. The output curve shows an increase of  $I_{\rm DS}$  current with increasing in positive (negative)  $V_{\rm DS}$  potential in Figure 2a,c. This is the behavior of an OECT device based on the variation of PANI conductivity through electrochemical doping/dedoping caused by the application of the gate potential. [50] The dependence of charge density or mobility, and consequently ionic conduction, with the applied gate potential,  $V_{\rm GS}$ , is responsible for the nonlinear increase of  $I_{\rm DS}$  with  $V_{\rm DS}$  and the absence of saturation regime. [51,52] For the transfer curves, the device's current,  $I_{\rm DS}$ , increases with an increase in negative (positive)  $V_{\rm GS}$  potential for a fixed positive (negative)  $V_{\rm DS}$  potential in Figure 2b,d.

The use of IDA microelectrodes for the PANI OECT device presented here afforded currents in the milliampere range that is higher than the current reported for other PANI-based transistors. The work by Kuo and co-workers<sup>[53]</sup> and the works by Li and co-workers in 2008<sup>[47]</sup> and 2013<sup>[48]</sup> showed solid-state PANI FETs with current in the microampere range while the work by Kuo

and Chiou<sup>[36]</sup> and the work by He and co-workers<sup>[50]</sup> presented the same kind of device with current in the nanoampere range. Regarding EGT, the work by Paul and co-workers<sup>[39]</sup> and the work by Alam and co-workers<sup>[40]</sup> presented PANI-based devices with the current in the microampere range. The intercalated drain and source electrodes in 65 pairs of the IDA microelectrode is responsible for the current amplification.

In the absence of a gate voltage,  $V_{GS} = 0$  V, current flows through the transistor channel at high  $V_{\text{DS}}$  potential, 3.0 V, in module, indicating that the device is in the ON state. The PANI OECT presents an  $I_{DS}$  of 1.9 mA at  $V_{\rm DS}$  = 3.0 V ( $V_{\rm GS}$  = 0 V) (Figure 2a,b) and an  $I_{\rm DS}$  of -1.9 mA at  $V_{\rm DS} = -3.0~{\rm V}~(V_{\rm GS} = 0~{\rm V})$  (Figure 2c,d). Once a positive gate bias is applied, the current decreases to 1.1 mA at  $V_{GS} = 0.5 \text{ V}$ , in Figure 2b, indicating a smooth depletionmode of operation. However, in Figure 2d, once a negative gate bias is applied, the current remains the same, -1.9 mA at  $V_{\rm GS}$  = -3.0 V. Nevertheless, once a negative (positive) gate bias is applied in the device in Figure 2b,d, the current increases (on-current of 3.9 mA at  $V_{\rm GS} = -$ 0.5 V and -3.5 mA at  $V_{\rm GS} = 0.5$  V, respectively), indicating an accumulation mode of operation with the injection of anions (cations) into the channel and a corresponding accumulation of holes (electrons).[17] For a lower drainsource potential,  $V_{\rm DS}$ , (2.0 and -2.0 V, Figures 2b and d, respectively) it is clear that the device works in accumulation operation mode.

The accumulation operation mode upon the application of both negative and positive gate voltages, with the conduction of both holes and electrons, indicates the ambipolar behavior for the PANI OECT devices. Thus, *p*-type PANI OECT device is demonstrated in Figure 2a,b, and *n*-type PANI OECT device in Figure 2c,d. The ambipolar behavior of PANI, arising from its electrochemical doping/dedoping process that is evaluated as reversible redox reaction, oxidation and reduction, was demonstrated by CV curves. The CV profile of PANI:DMF thin film is shown in the inset of Figure 2c. From the CV graph, it is possible to observe a reversible electrochemical switching between the reduced and the oxidized states of PANI in the electrochemical window of OECT operation (from -0.5 to 0.5 V).

To verify the doping/dedoping process as a consequence of the injection of ions from the electrolyte into the OSC layer of the transistor, the PANI-based device in sodium phosphate buffer (PB) and DI-water (DI-W), without ions, were compared. The transfer curves for  $V_{\rm GS}$  from -0.4 to 0.5 V, at  $V_{\rm DS}=3.0$  V, are shown in Figure 3. The device operating with PB (PANI OECT PB) presents modulation of its drain-source current,  $I_{\rm DS}$ , with increasing gate voltage,  $V_{\rm GS}$ , while the device operating in DI-W (PANI OECT DI-W) does not present modulation. These results

ns) on Wiley Online Library for rules of use; OA articles are governed by the applicable Creative Commons

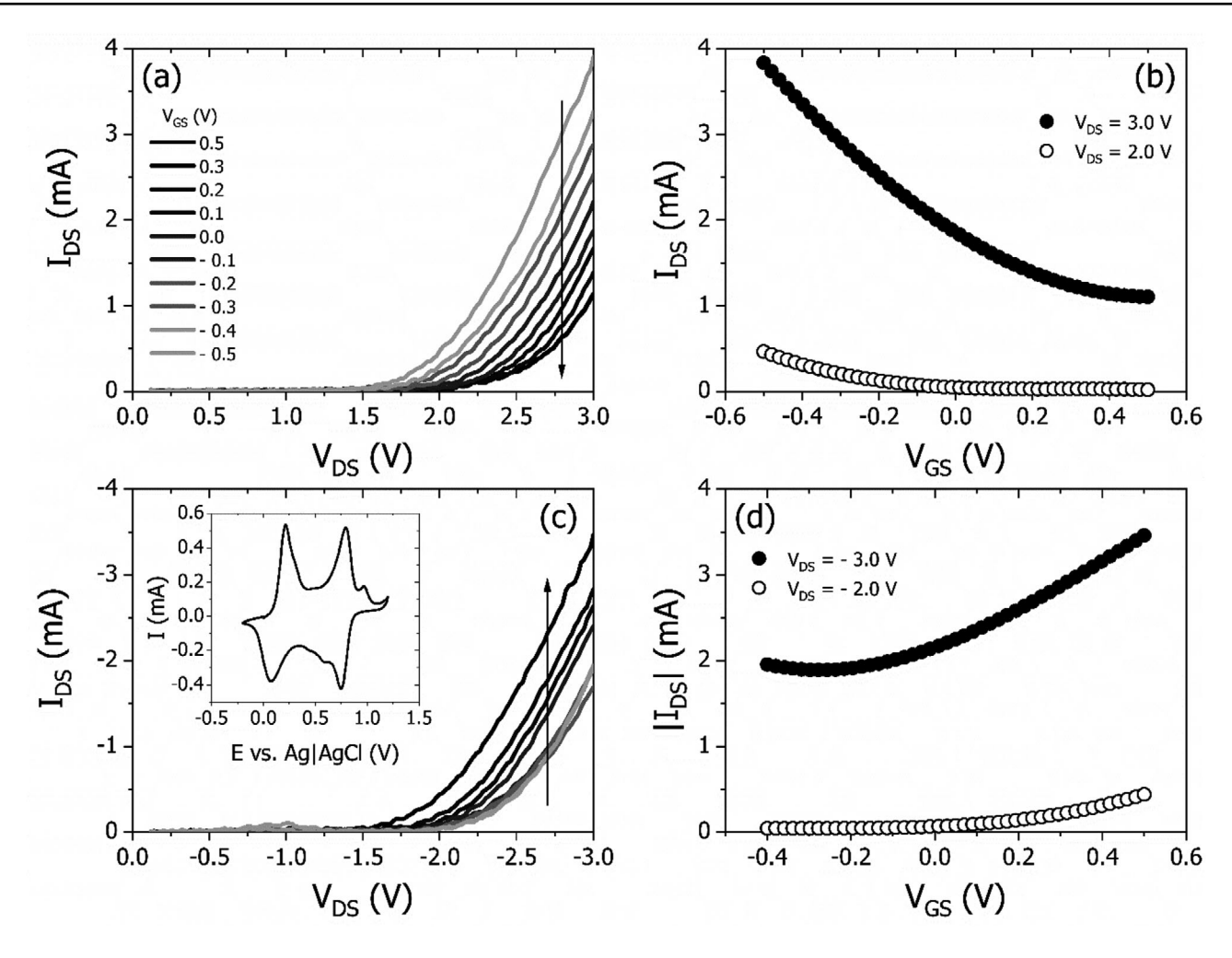


FIGURE 2 Performance of the ambipolar PANI OECT. (a) p-type output characteristics, (b) p-type transfer curve at  $V_{\rm DS} = 3.0$  V (black dots) and at 2.0 V (hollow dots), (c) n-type output characteristics, and (d) n-type transfer curve at  $V_{\rm DS} = -0.3$  V (black dots) and -2.0 V (hollow dots), measured in 0.5 mol/L sodium phosphate buffer (PB). The  $V_{\rm GS}$  range is from -0.5 to 0.5 V in a 0.1  $V_{\rm GS}$  step. The inset is the CV profile for the PANI:DMF film

indicate that PANI OECT device is based on doping/dedoping by ion injection into the polymeric layer. [17]

As shown by Meijer and co-workers, the ambipolar transport is observed on reduction of the injection barriers for holes and electrons into the semiconductor, by applying both a drain-source and a gate-source potential simultaneously, helping the modulation of the device, and by using low bandgap semiconductors. [56] Besides the clear combination of  $V_{\rm DS}$  and  $V_{\rm GS}$  in the operation of the PANI-based OECT shown, the bandgap energy for PANI-EB is estimated around 0.90 eV, [57] which is approximately 0.65 eV lower than the poly(3,9-di-t-butylindeno[1,2-b] fluorene) (PIF) bandgap, around 1.55, reported as the OSC in an organic ambipolar transistor by Meijer and co-workers.

The acid-doped PANI presents increased conductivity when compared to the undoped PANI due to protonation of the polymeric structure. [58–61] An acid-doped PANI OECT (PANI:DMF:HCl) was evaluated in the PB

electrolyte and compared to the undoped PANI OECT (PANI:DMF). The transfer curves of the p-type and n-type devices are shown in Figure 4a and b, respectively. The PANI:DMF:HCl device presented increased  $I_{\rm DS}$ , compared to the PANI:DMF device, around 17 %, for p-type, reaching  $I_{\rm DS}=3.9$  mA ( $V_{\rm GS}=-0.4$  V), and around of 38%, for n-type, reaching  $I_{\rm DS}=4.8$  mA ( $V_{\rm GS}=0.5$  V). Enhanced drainsource currents for HCl-doped PANI FET devices were presented by Kuo and co-workers. [53] The higher current for doped PANI OECT is related to its narrower bandgap, estimated around 0.50 eV, [57] which is lower than that of undoped PANI-EB and ensures a lower injection barrier for ambipolar devices, as discussed. Thus, an acid doped PANI facilitates the injection of ions from the electrolyte, increasing the  $I_{\rm DS}$  current.

The UV-Vis absorption spectra of the deposition solution for PANI:DMF and PANI:DMF:HCl are shown in Figure 5a. The UV-Vis spectra are indicative of the doping

doi/10.1002/elsa.202100176 by University Of Sao Paulo - Brazil, Wiley Online Library on [16/10/2025]. See the Terms

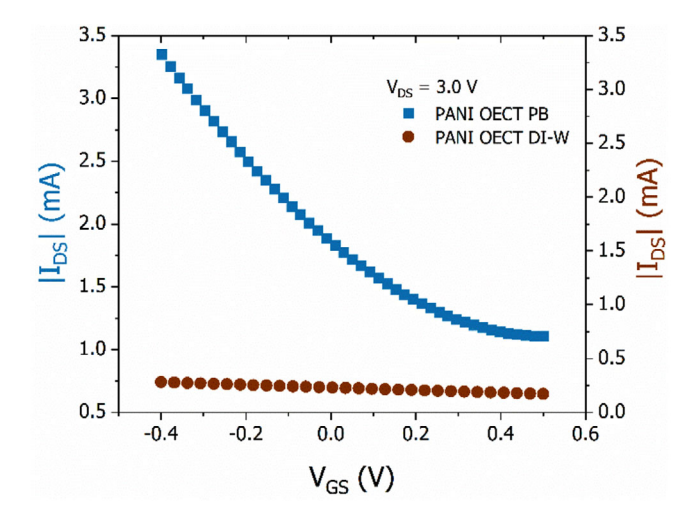
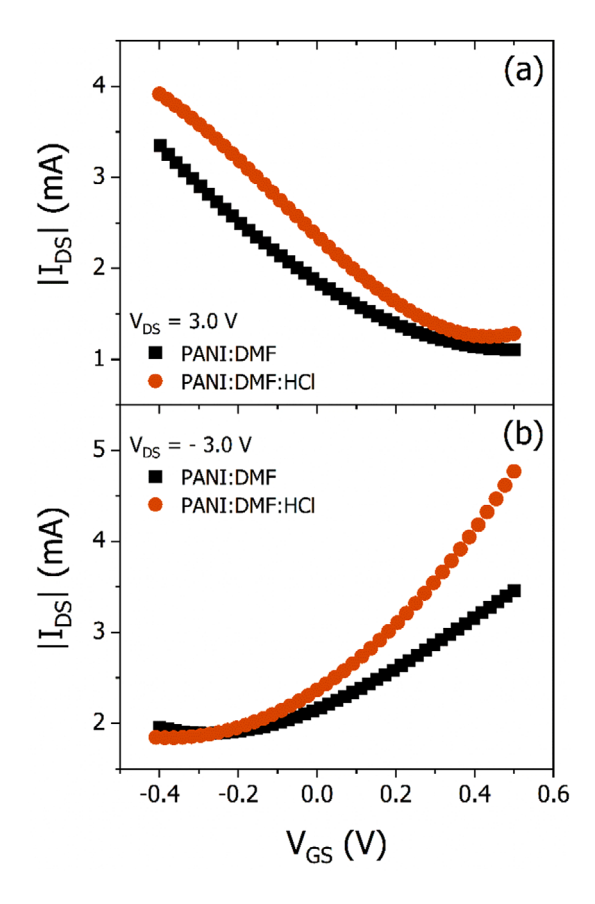


FIGURE 3 Comparison of OECT performance as function of electrolyte. The PANI OECT PB device (blue-square symbols) operating in sodium phosphate buffer presented increasing  $I_{\rm DS}$  with increasing negative  $V_{\rm GS}$  potential while the PANI OECT DI-W device (brown-circle symbols) presented no significant change in the  $I_{\rm DS}$  with  $V_{\rm GS}$  variation



**FIGURE 4** Comparison of undoped and doped PANI OECT. (a) *p*-type transfer curves for undoped (PANI:DMF) and doped (PANI:DMF:HCl) OECT devices and (b) *n*-type transfer curves for undoped and doped OECT devices. Acid doping of PANI causes a decrease in bandgap and a consequent decrease in the injection barrier, facilitating the ambipolar device performance

level of PANI samples and the acid doped PANI (protonated) can be distinguished from the undoped PANI samples. The protonated PANI are green [62] and present absorption band at longer wavelengths of the visible spectra which reflects the presence of polarons on its structure, as can be seen for PANI:DMF:HCl spectra in Figure 5. This indicates a protonated and conductive PANI. [63] The undoped PANI presents a peak around 600 nm that shifts to approximately 800 nm (the absorption band at longer wavelengths) after protonation, as observed in the literature. [63] The UV-Vis spectrum of PANI:DMF:HCl also presents a peak located between 350 and 500 nm indicative of a  $\pi$ - $\pi$ \* transition. [35]

The facilitated electrochemical doping/dedoping of the HCl-doped PANI when compared to the undoped PANI can be seen by CV curves of PANI:DMF and PANI:DMF:HCl, shown in Figure 5b. The CV indicates a more pronounced reversible electrochemical switching between the reduced and oxidized states of PANI, which can be seen by an increase in the oxidation and reducing peak currents, for the PANI:DMF:HCl in the electrochemical window of OECT operation. The CV profile is similar for PANI samples but the current increased five times, approximately, for the doped PANI. This increase in electrochemical doping/dedoping by injection of ions from the electrolyte causes an increase in PANI conductivity, changing the OECT modulation as shown in Figure 4.

To compare the OECT performance with the other EGT described, the EGOFET, we evaluated the P3HT-based EGOFET using IDA microelectrode. The output and transfer curves for the P3HT-based EGOFET with DI-water as electrolyte, gated via Pt rod, are shown in Figure 6. The P3HT-based EGOFET present an opposite behavior compared to the PANI-based OECT, that is, for negative drain-source polarity, the  $I_{\rm DS}$  increases with increasing negative gate,  $V_{GS}$ , voltage, which is in agreement with the field-effect modulation.<sup>[5,64]</sup> The device presented on-current of about ~350  $\mu$ A, with  $V_{\rm DS}$  = -0.4 V, saturation regime, and  $V_{\rm GS} = -0.3$  V. This is approximately 3 orders of magnitude larger than single drain-source contact based device, as presented in the literature. [65-68] P3HT-based devices with IDA microelectrodes reported in literature also presented the same current range. [69] The transfer curve in linear regime,  $V_{\rm DS}$  = - 0.1 V, is also shown in Figure 6b.

These results clearly demonstrate the difference in the operation mode of a PANI-based OECT and a P3HT-based EGOFET, both fabricated using an IDA microelectrode. The PANI OECT operates based on the injection of ions from the electrolyte into the OSC layer, responsible for modulating the charges in the channel and the drain-source current, as consequence. When the PANI EGT was tested in DI-water, no modulation in current was noticed

Wiley Online Library on [16/10/2025]

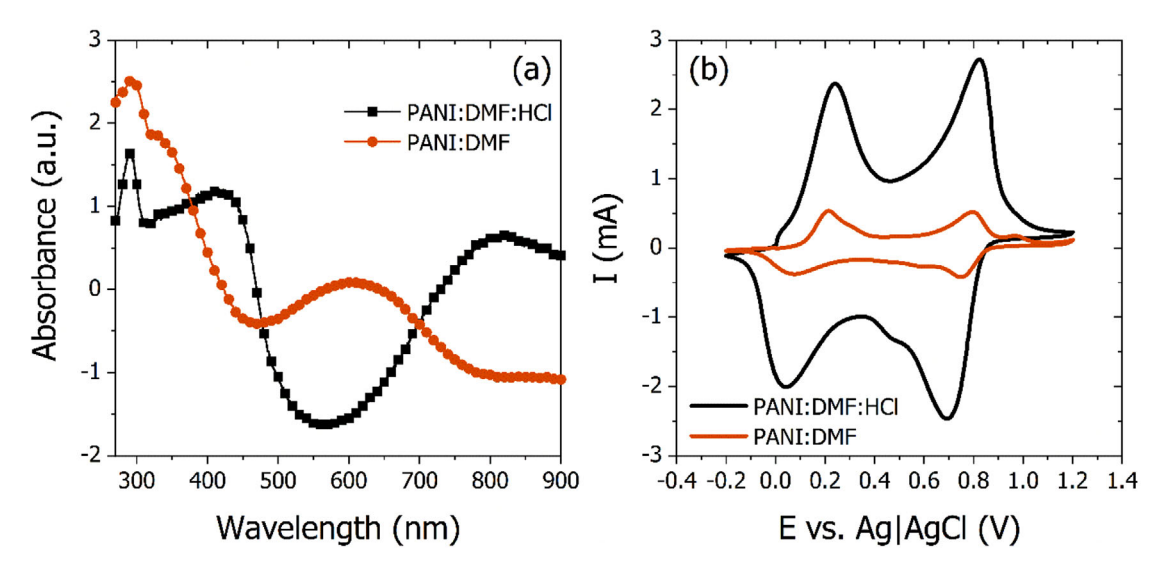


FIGURE 5 UV-Vis absorption spectra of deposition solution of PANI:DMF and PANI:DMF:HCl samples in panel (a). The shifted peaks of absorption from PANI:DMF to PANI:DMF:HCl are observed upon protonation. Cyclic voltammetry of PANI doped and undoped thin films in panel (b). The PANI:DMF and PANI:DMF:HCl were deposited by spin coating on FTO substrates and measured with a scan rate of 50 mV/s

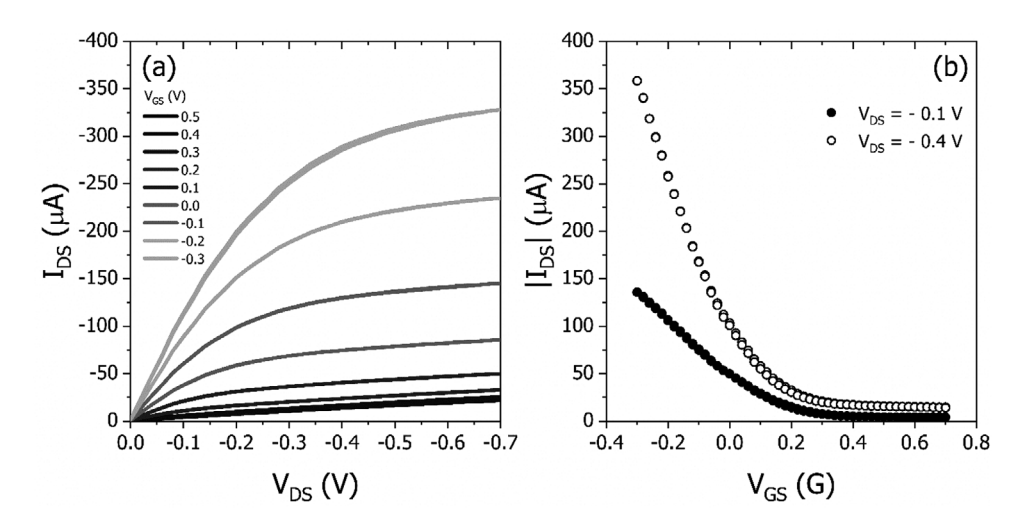


FIGURE 6 Performance of the *p*-type P3HT EGOFET with Pt rod gate electrode. (a) The output characteristic, (b) the transfer curve at linear,  $V_{\rm DS} = -0.1$  V, (black dots) and saturation,  $V_{\rm DS} = -0.4$  V, (hollow dots) regimes, measured in deionized water. The  $V_{\rm GS}$  range is from -0.3 to 0.7 V in a 0.1 V<sub>GS</sub> step

probably due to the low gate and drain voltages (lower than 1 V) (solid-state PANI-based FET devices were reported for  $V_{\rm DS}$  and  $V_{\rm GS}$  in the range of tens of volts<sup>[36,37]</sup>) and the impossibility of the formation of the conduction channel other than by electrochemical doping once PANI is an electrically conducting polymer. To obtain an EGOFET device operating in a range lower than 1 V, the need is for polymeric layers able to form a conduction channel without ion injection, and it was demonstrated with the use of P3HT that is hydrophobic with negligible ion penetration and electrochemical reactions within a certain potential window. [70,71]

### 4 | CONCLUSIONS

We demonstrated a functional ambipolar OECT fabricated with spin-coated PANI thin films operating in a buffer electrolyte and gated via Pt rods. The electrolyte-gated device relies on the electrochemical doping/dedoping of the OSC layer in the OTFT structure that is obtained with PANI once it undergoes reversible redox reaction, oxidation and reduction, in the electrochemical window of transistor operation. The ambipolar PANI OECT exhibits a good overall performance with on-currents up to  $I_{\rm DS}=3.5~{\rm mA}$ , approximately. An HCl-doped PANI was used as OSC layer

in the OECT architecture to evaluate the effect on the device's performance. The PANI:DMF:HCl transistor presented increased on-current around 17% ( $I_{DS} = 3.9 \text{ mA}$ ) for p-type and around 38% ( $I_{DS} = 4.8 \text{ mA}$ ) for n-type operations. This current increase can be justified by the decrease in polymer bandgap that decreases the injection barrier. Evaluation of device performance with DI-water as electrolyte was accomplished for PANI-based OECT and P3HT-based EGOFET where the former did not present current modulation, unlike the last. Device architecture, the IDA microelectrode, allows for increased drain-source current due to the larger active area for the device when compared to single drain-source contact substrates. In proper conditions, PANI is able to perform as ambipolar OECT, which may open new possibilities for bio- and ionsensors devices.

### ACKNOWLEDGMENTS

The authors would like to thank the Photobiophysics Group from the Department of Physics of the FFCLRP/USP for experimental help. This work was funded by Coordenação de Aperfeiçoamento de Pessoal de Nível Superior (CAPES), Fundação de Amparo à Pesquisa do Estado de São Paulo (FAPESP, 2018/24395-8, 2018/22223-5, 2017/24201-6, and 2014/24559-0) and Conselho Nacional de Desenvolvimento Científico e Tecnológico (CNPq, 308713/2018-4) Brazilian agencies.

### CONFLICT OF INTEREST

The authors have declared np conflict of interest.

### DATA AVAILABILITY STATEMENT

The data that support the findings of this study are available from the corresponding author upon reasonable request.

### ORCID

Hugo José Nogueira Pedroza Dias Mello https://orcid.org/0000-0003-2676-3826

### REFERENCES

- 1. J. E. Lilienfeld, Method and Apparatus for Controlling Electric Currents, **1930**, US1745175A.
- S. M. Sze, K. K. Ng, Physics of Semiconductor Devices, Wiley-Interscience, 2006.
- 3. R. A. Street, Adv. Mater 2009, 21, 2007.
- 4. L. Torsi, Microelectron, Reliab 2000, 40, 779.
- 5. G. Horowitz, J. Mater. Res 2004, 19, 1946.
- 6. H. Du, X. Lin, Z. Xu, D. Chu, J. Mater. Sci 2015, 50, 5641.
- 7. D. Tu, L. Herlogsson, L. Kergoat, X. Crispin, M. Berggren, R. Forchheimer, *IEEE Trans. Electron Devices* **2011**, *58*, 3574.
- 8. H. Yuan, H. Shimotani, A. Tsukazaki, A. Ohtomo, M. Kawasaki, Y. Iwasa, *J. Am. Chem. Soc* **2010**, *132*, 6672.

- L. Kergoat, B. Piro, M. Berggren, G. Horowitz, M.-C. Pham, Anal. Bioanal. Chem 2012, 402, 1813.
- L. Kergoat, L. Herlogsson, D. Braga, B. Piro, M.-C. Pham, X. Crispin, M. Berggren, G. Horowitz, Adv. Mater 2010, 22, 2565.
- F. Buth, A. Donner, M. Sachsenhauser, M. Stutzmann, J. A. Garrido, Adv. Mater 2012, 24, 4511.
- L. Torsi, M. Magliulo, K. Manoli, G. Palazzo, *Chem. Soc. Rev* 2013, 42, 8612.
- 13. K. Melzer, M. Brändlein, B. Popescu, D. Popescu, P. Lugli, G. Scarpa, *Faraday Discuss* **2014**, *174*, 399.
- 14. D. Wang, V. Noël, B. Piro, Electronics 2016, 5, 9.
- A. Laiho, L. Herlogsson, R. Forchheimer, X. Crispin, M. Berggren, Proc. Natl. Acad. Sci 2011, 108, 15069.
- D. Khodagholy, J. Rivnay, M. Sessolo, M. Gurfinkel, P. Leleux, L. H. Jimison, E. Stavrinidou, T. Herve, S. Sanaur, R. M. Owens, G. G. Malliaras. *Nat. Commun* 2013, 4, 2133.
- 17. J. Rivnay, S. Inal, A. Salleo, R. M. Owens, M. Berggren, G. G. Malliaras, *Nat. Rev. Mater* **2018**, *3*, 1.
- J. T. Friedlein, R. R. McLeod, J. Rivnay, Org. Electron 2018, 63, 398.
- 19. C. Bartic, A. Campitelli, S. Borghs, Appl. Phys. Lett 2003, 82, 475.
- S. M. Goetz, C. M. Erlen, H. Grothe, B. Wolf, P. Lugli, G. Scarpa, Org. Electron 2009, 10, 573.
- S. Casalini, F. Leonardi, T. Cramer, F. Biscarini, Org. Electron 2013, 14, 156.
- M. Berto, S. Casalini, M. Di Lauro, S. L. Marasso, M. Cocuzza,
   D. Perrone, M. Pinti, A. Cossarizza, C. F. Pirri, D. T. Simon, M.
   Berggren, F. Zerbetto, C. A. Bortolotti, F. Biscarini, *Anal. Chem* 2016, 88, 12330.
- M. Berto, C. Diacci, R. D'Agata, M. Pinti, E. Bianchini, M. Di Lauro, S. Casalini, A. Cossarizza, M. Berggren, D. Simon, G. Spoto, F. Biscarini, C. A. Bortolotti, *Adv. Biosyst* 2017, 2, 1700072.
- N. Wang, A. Yang, Y. Fu, Y. Li, F. Yan, Acc. Chem. Res 2019, 52, 277.
- 25. P. N. Bartlett, P. R. Birkin, Anal. Chem 1993, 65, 1118.
- 26. P. Lin, F. Yan, Adv. Mater 2012, 24, 34.
- X. Strakosas, M. Bongo, R. M. Owens, J. Appl. Polym. Sci 2015, 132, https://doi.org/10.1002/app.41735
- L. Chen, Y. Fu, N. Wang, A. Yang, Y. Li, J. Wu, H. Ju, F. Yan, ACS Appl. Mater. Interfaces 2018, 10, 18470.
- 29. B. Piro, G. Mattana, S. Zrig, G. Anquetin, N. Battaglini, D. Capitao, A. Maurin, S. Reisberg, Appl. Sci 2018, 8, 928.
- T. Cramer, A. Campana, F. Leonardi, S. Casalini, A. Kyndiah, M. Murgia, F. Biscarini, J. Mater. Chem. B 2013, 1, 3728.
- 31. T. Fujimoto, K. Awaga, Phys. Chem. Chem. Phys 2013, 15, 8983.
- 32. D. A. Bernards, G. G. Malliaras, Adv. Funct. Mater 2007, 17, 3538.
- J. Rivnay, P. Leleux, M. Ferro, M. Sessolo, A. Williamson, D. A. Koutsouras, D. Khodagholy, M. Ramuz, X. Strakosas, R. M. Owens, C. Benar, J.-M. Badier, C. Bernard, G. G. Malliaras, Sci. Adv 2015, 1, e1400251.
- 34. J. Zaumseil, H. Sirringhaus, Chem. Rev 2007, 107, 1296.
- A. Giovannitti, C. B. Nielsen, D.-T. Sbircea, S. Inal, M. Donahue, M. R. Niazi, D. A. Hanifi, A. Amassian, G. G. Malliaras, J. Rivnay, I. McCulloch, *Nat. Commun* 2016, 7, 13066.
- 36. C.-T. Kuo, W.-H. Chiou, Synth. Met 1997, 88, 23.
- C.-T. Kuo, S.-A. Chen, G.-W. Hwang, H.-H. Kuo, Synth. Met 1998, 93, 155.
- H. J. N. P. D. Mello, M. Mulato, J. Appl. Polym. Sci 2018, 135, 46625.

Chemistry

- 39. E. W. Paul, A. J. Ricco, M. S. Wrighton, J. Phys. Chem 1985, 89,
- 40. M. M. Alam, J. Wang, Y. Guo, S. P. Lee, H.-R. Tseng, J. Phys. Chem. B 2005, 109, 12777.
- 41. L. Travaglini, A. P. Micolich, C. Cazorla, E. Zeglio, A. Lauto, D. Mawad, Adv. Funct. Mater 2021, 31, 2007205.
- 42. E. M. Genies, C. Tsintavis, J. Electroanal. Chem. Interfacial Electrochem 1985, 195, 109.
- 43. Z. Ping, B. G. E. Nauer, H. Neugebauer, J. Theiner, A. Neckel, J. Chem. Soc. Faraday Trans 1997, 93, 121.
- 44. J. E. Albuquerque, L. H. C. Mattoso, D. T. Balogh, R. M. Faria, J. G. Masters, A. G. MacDiarmid, Synth. Met 2000, 113, 19.
- 45. M. M. Mahat, D. Mawad, G. W. Nelson, S. Fearn, R. G. Palgrave, D. J. Payne, M. M. Stevens, J. Mater. Chem. C 2015, 3, 7180.
- 46. H. J. N. P. D. Mello, T. Heimfarth, M. Mulato, Mater. Chem. Phys 2015, 160, 257,
- 47. Y.-C. Li, Y.-J. Lin, H.-J. Yeh, T.-C. Wen, L.-M. Huang, Y.-K. Chen, Y.-H. Wang, Appl. Phys. Lett 2008, 92, 093508.
- 48. Y.-C. Li, Y.-J. Lin, C.-Y. Wei, Y.-H. Wang, Solid-State Electron 2013, 79, 56.
- 49. K. Chatterjee, P. Dhara, S. Ganguly, K. Kargupta, D. Banerjee, Sens. Actuators B Chem 2013, 181, 544.
- 50. H. X. He, C. Z. Li, N. J. Tao, Appl. Phys. Lett 2001, 78, 811.
- 51. X. L. Chen, Z. Bao, J. H. Schön, A. J. Lovinger, Y.-Y. Lin, B. Crone, A. Dodabalapur, B. Batlogg, Appl. Phys. Lett 2001, 78, 228.
- 52. D. Nilsson, M. Chen, T. Kugler, T. Remonen, M. Armgarth, M. Berggren, Adv. Mater 2002, 14, 51.
- 53. C.-T. Kuo, S.-Z. Weng, R.-L. Huang, Synth. Met 1997, 88, 101.
- 54. S. Pruneanu, E. Veress, I. Marian, L. Oniciu, J. Mater Sci. 1999, 34, 2733.
- 55. C. Kaneda, Y. Sueyasu, E. Tanaka, M. Atobe, Ultrason. Sonochem **2020**, *64*, 104991.
- 56. E. J. Meijer, D. M. de Leeuw, S. Setayesh, E. van Veenendaal, B.-H. Huisman, P. W. M. Blom, J. C. Hummelen, U. Scherf, T. M. Klapwijk, Nat. Mater 2003, 2, 678.

- 57. Y. Mu, Y. Xie, J. Phys. Chem. C 2019, 123, 18232.
- 58. J.-C. Chiang, A. G. MacDiarmid, Synth. Met 1986, 13, 193.
- 59. A. G. Macdiarmid, J. C. Chiang, A. F. Richter, A. J. Epstein, Synth. Met 1987, 18, 285.
- 60. J. Stejskal, D. Hlavatá, P. Holler, M. Trchová, J. Prokeš, I. Sapurina, Polym. Int 2004, 53, 294.
- 61. H. J. N. P. D. Mello, M. Mulato, Thin Solid Films 2018, 656, 14.
- 62. H. J. N. P. D. Mello, M. Mulato, Sens. Actuators B Chem 2015, 213, 195.
- 63. N. V. Blinova, I. Sapurina, J. Klimovič, J. Stejskal, Polym. Degrad. Stab 2005, 88, 428.
- 64. G. Horowitz, Adv. Mater 1998, 10, 365.
- 65. L. Kergoat, B. Piro, M. Berggren, M.-C. Pham, A. Yassar, G. Horowitz, Org. Electron 2012, 13, 1.
- 66. C. Suspène, B. Piro, S. Reisberg, M.-C. Pham, H. Toss, M. Berggren, A. Yassar, G. Horowitz, J. Mater. Chem. B 2013, 1, 2090.
- 67. S. Han, X. Zhuang, W. Shi, X. Yang, L. Li, J. Yu, Sens. Actuators B Chem 2016, 225, 10.
- 68. H. J. N. P. D. Mello, S. Dalgleish, G. Ligorio, M. Mulato, E. J. W. List-Kratochvil, in Org. Hybrid Sens. Bioelectron. XI, International Society For Optics And Photonics, 2018, p. 1073819.
- 69. K. Melzer, A. M. Münzer, E. Jaworska, K. Maksymiuk, A. Michalska, G. Scarpa, Org. Electron 2014, 15, 595.
- 70. O. Larsson, A. Laiho, W. Schmickler, M. Berggren, X. Crispin, Adv. Mater 2011, 23, 4764.
- 71. K. Schmoltner, J. Kofler, A. Klug, E. J. W. List-Kratochvil, in Proc SPIE, 2013, pp. 88311N-88311N-12.

How to cite this article: H. J. N. P. D. Mello, M. C. Faleiros, M. Mulato, Electrochem Sci Adv. 2022, 2, e2100176. https://doi.org/10.1002/elsa.202100176